WM2017 Conference, March 5-9, 2017, Phoenix, Arizona, USA.

Effect of Silica Particle Size on Nuclear Waste-to-Glass Conversion – 17319

Derek R. Dixon*, Derek Cutforth*, Brad VanderVeer*, Michael J. Schweiger*, and Pavel Hrma*

*Pacific Northwest National Laboratory, Richland, WA 99354, derek.dixon@pnnl.gov

ABSTRACT

The process for converting nuclear waste-to-glass in an electric melter occurs in the cold cap, a crust of reacting solids floating on the glass pool. As the melter feed (a mixture of the nuclear waste and glass forming and modifying additives) heats up in the cold cap, glass-forming reactions ensue, causing the feed matrix to connect, trapping reaction gases to create a foam layer. The foam layer reduces the rate of melting by separating the reacting feed from the melt pool. The size of the silica particle additives in the melter feed affects melt viscosity and, hence, foam stability. To investigate this effect, seven nuclear waste simulant feeds of a high-level waste were batched as slurries and prepared with dissimilar ranges of silica particle size. Each slurry feed was charged into a laboratory-scale melter (LSM) to produce a cold cap and the propensity of feeds to foam was determined by pressing dried feeds into pellets and monitoring the change of pellet volume in response to heating. Two of these slurries were designed to have dissimilar glass viscosities at 1150°C. In the low temperature region of the cold cap, before the melter feed connects, the feeds without fine silica particles behaved similar to the high viscosity feed as their volume contracted while the feed with silica particles no larger than 5 µm reacted like the low viscosity feed. However, the feed volume similarities reversed as the feed connected and expanded through the foam region of the cold cap.

INTRODUCTION

The Hanford site in Eastern Washington State contains 210,000 m^3 of nuclear waste stored in 177 underground tanks, a result of the production of plutonium from 1943-1987 [1, 2]. To immobilize this waste, the Hanford Tank Waste Treatment and Immobilization Plant (WTP) is being constructed onsite where the waste will be combined with glass forming and modifying additives (GFMAs) and fed into electric melters for vitrification [1, 2]. The Department of Energy Office of River Protection has developed an integrated program to increase the waste loading into glass while meeting the melter lifetime, process, regulatory, and product requirements for the WTP [3]. One section of this program focuses on increasing the glass production rate in the melters, which can be achieved by increasing the melting rate of the glass [3].

The melting process for converting melter feed (a mixture of the nuclear waste and GFMAs) to glass occurs in the cold cap, a crust of reacting solids floating on the molten glass pool in an electric melter [4]. As the melter feed heats up in the cold cap, glass-forming reactions ensue, causing the feed matrix to connect (typically

>800°C) and trap the reaction gases within the transient melt to create a foam layer that separates the reacting feed from the melt pool thus restricting the heat flow and reducing the rate of melting [4, 5]. Foam bubbles coalesce into cavities that travel horizontally and escape around the edges of the cold cap into the melter plenum space [5, 6].

One of the components that play a role in the formation of the foam layer is the silica, granular quartz, which is added to the melter feed as a part of the GFMAs. The size of the silica particles affects their dissolution rate in the glass-forming melt and, hence, the melt viscosity [7-9]. The glass melt viscosity is a function of both temperature and composition, which are both varying in the foam layer (700°C – 1050°C) as different sized silica dissolves at different rates affecting the melt composition [9]. The size of silica particles in the melt is one of the factors that affect the foam stability [6, 7, 9, 10].

To investigate the effect of silica particle size, seven nuclear waste simulant feeds were batched as slurries. All slurry feeds encompassed a simplified, high-alumina, high-level waste (HLW) composition. Five slurries were prepared with dissimilar ranges of silica particle size and two slurries were designed to have different glass viscosities at 1150°C with minimal composition variation from the original. Each slurry feed was charged into a laboratory-scale melter (LSM) to produce a cold cap. During charging, the spread of slurry on the cold cap and the movement of gas cavities in the glass melt were observed. After charging for a fixed time, the cold cap was preserved by rapid cooling and then cross-sectioned for image analysis. The propensity of feeds to foam was determined by pressing dried feeds into pellets and monitoring the change of pellet volume in response to heating.

EXPERIMENTAL METHODS

A19 Feed Composition

The glass used in this study was a HLW simulant adapted from the HWI-Al-19 with 45% waste loading formulation used in previous small-scale melter tests [11]. The adjusted composition, referred to here as A19, removed several of the trace oxides (BaO, CdO, K_2O, MgO, TiO_2, and ZnO), and the final A19 glass oxide composition is shown in TABLE I. The viscosity of the A19 glass at 1150°C was measured as previously discussed [6, 7] and is shown in TABLE I.

Composition Variations

The amounts of B_2O_3, Li_2O, Na_2O, and SiO_2 in the A19 glass were adjusted to generate two additional glass compositions with varying viscosities at 1150°C. One of these compositions, referred to as A19-1, was adjusted to have a calculated viscosity less than that of the original A19 glass. The other composition, referred to as A19-9, was adjusted to have a calculated viscosity greater than that of A19. The original and modified compositions as well as their measured viscosity values are shown in TABLE I.

TABLE I. A19, A19-1, and A19-9 Glass Composition (in Mass Fractions) and the Oxide Feed Components (g) for 1 g of Glass

Glass	A19-1	A19	A19-9	Oxide Feed	A19-1	A19	A19-9
Al_2O_3	0.2420	0.2420	0.2420	$Al(OH)_3$	0.3703	0.3703	0.3703
B_2O_3	0.2140	0.1919	0.1660	H_3BO_3	0.3801	0.3409	0.2949
Bi_2O_3	0.0116	0.0116	0.0116	Bi_2O_3	0.0116	0.0116	0.0116
CaO	0.0559	0.0559	0.0559	$CaCO_3$	0.0997	0.0997	0.0997
Cr_2O_3	0.0053	0.0053	0.0053	Cr_2O_3	0.0053	0.0053	0.0053
F	0.0067	0.0067	0.0067	NaF	0.0149	0.0149	0.0149
Fe_2O_3	0.0596	0.0596	0.0596	Fe_2O_3	0.0596	0.0596	0.0596
Li_2O	0.0398	0.0357	0.0309	Li_2CO_3	0.0985	0.0883	0.0764
Na_2O	0.1072	0.0961	0.0832	Na_2CO_3	0.1539	0.1350	0.1128
NiO	0.0040	0.0040	0.0040	NiO	0.0040	0.0040	0.0040
P_2O_5	0.0106	0.0106	0.0106	$NaPO_3$	0.0153	0.0153	0.0153
PbO	0.0041	0.0041	0.0041	PbO	0.0041	0.0041	0.0041
SiO_2	0.2332	0.2704	0.3141	SiO_2	0.2332	0.2704	0.3141
SO_3	0.0020	0.0020	0.0020	Na_2SO_4	0.0036	0.0036	0.0036
ZrO_2	0.0040	0.0040	0.0040	ZrO_2	0.0040	0.0040	0.0040
Sum	1.0000	1.0000	1.0000	Sum	1.4580	1.4270	1.3905
Viscosity @ 1150°C (Pa s)	1.94	3.64	8.49				

Silica Partitions

Five fractions of silica particle sizes were prepared for the feed by sifting the silica source given in TABLE II to the range of particle sizes listed. The term “fines” refers to silica particles less than 5 µm.

TABLE II. Silica Fraction Particle Sizes

Silica Fraction Title	Minimum Particle (µm)	Maximum Particle (µm)	Source
5	Fines	5	Min-U-Sil 5
45	Fines	45	Sil-Co-Sil 75
75	Fines	75	Sil-Co-Sil 75
45-75	45	75	Sil-Co-Sil 75
75-106	75	106	Sil-Co-Sil 106

Laboratory-Scale Melter Runs

Seven slurry feeds, shown in TABLE III, were prepared for LSM runs using the feed compositions and silica fractions listed. For the three feeds with the silica partitions from fines to 75 µm (A191_75, A19_75, and A199_75), the feed chemicals (TABLE IV) to make 250 g of glass were added to deionized water up to a total volume of 500 mL to produce a final feed slurry concentration of 500 g L^{-1}. For the remaining

four feeds (A19_5, A19_45, A19_45-75, and A19_75-106), the feed chemicals (TABLE IV) to make 400 g of glass were added to deionized water up to a total volume of 1000 mL to produce a final feed slurry concentration of 400 g L^{-1}.

TABLE III Feed Characteristics

Feed Name	Feed Composition	Silica Fraction
A191_75	A19-1	75
A19_75	A19	75
A199_75	A19-9	75
A19_5	A19	5
A19_45	A19	45
A19_45-75	A19	45-75
A19_75-106	A19	75 -106

TABLE IV. A19, A19-1, and A19-9 Slurry Feed Components (g) for 1 g of Glass

Slurry Feed	A19-1	A19	A19-9
$Al(OH)_3$	0.3718	0.3718	0.3718
H_3BO_3	0.3809	0.3416	0.2955
Bi_2O_3	0.0117	0.0117	0.0117
CaO	0.0109	0.0109	0.0109
$Cr_2O_3 \cdot 1.5H_2O$	0.0062	0.0062	0.0062
NaF	0.0150	0.0150	0.0150
$Fe(OH)_3$	0.0744	0.0744	0.0744
Li_2CO_3	0.0995	0.0892	0.0772
$Ni(OH)_2$	0.0050	0.0050	0.0050
$Fe(H_2PO_2)_3$	0.0125	0.0125	0.0125
PbO	0.0042	0.0042	0.0042
SiO_2	0.1910	0.2214	0.2572
Na_2SO_4	0.0036	0.0036	0.0036
$Zr(OH)_4$	0.0055	0.0055	0.0055
$CaSiO_3$	0.0971	0.0971	0.0971
NaOH	0.0199	0.0199	0.0199
Na_2CO_3	0.1188	0.1066	0.0922
$NaNO_2$	0.0035	0.0035	0.0035
$NaNO_3$	0.0124	0.0124	0.0124
$Na_2C_2O_4$	0.0013	0.0013	0.0013
Sum	1.4450	1.4137	1.3769

For each feed, an LSM crucible was loaded with 200 g of glass corresponding to the feed composition and placed in the 1200°C LSM furnace as previously described [6, 12-15]. For the A191_75, A19_75, and A199_75 LSM runs, the feed slurries were charged at a rate of 6.5 mL min^{-1} for a run time of 35 minutes and the A19_5, A19_45, A19_45-75, and A19_75-106 feed slurries were charged at a rate of 8.2 mL min^{-1} for a run time of 35 minutes. The difference in charging rate ensured that runs with different glass yields of the slurries achieved an effective glass production rate of 660 kg m^{-2} day^{-1} in the cross-sectional area of the LSM melter (70.9 cm^2).

At the end of the charging time, the crucible was removed from the LSM furnace and quenched on a copper block. Pictures and video were taken of the slurry spreading on the cold cap and gas cavities bursting around the cold cap in 5 minute intervals up to minute 30 of the run. After cooling, the cold caps were split along existing fracture surfaces for optical imaging.

Volume Expansion Test

A19, A19-1, and A19-9 feed slurries were batched without silica, dried to a solid, and ground to a powder. A pellet of each feed in TABLE III was prepared by adding the appropriate fraction of silica to the powdered slurry, mixing the two, and pressing the powder into a 1.5 g, 13-mm diameter, and 6-mm tall pellet. Each pellet was heated at 10 K min^{-1} from room temperature to 1090°C. The expansion of pellets was photographically documented. The pellet profile area was determined by image analysis and the volume (V) was obtained via numerical integration [7, 16, 17]. The normalized bulk volume (V/V_0), where V_0 is the initial pellet volume, was plotted as a function of temperature. The experiment was repeated three times for each feed.

RESULTS AND DISCUSSION

The feed volume expansion for the glass viscosity variation series (A191_75, A19_75, and A199_75) is displayed in Fig. 1a. During the volume decreasing temperature range of ~540°C-715°C, depending on the feed, the feed contracted as the early-melting components (primarily B_2O_3, Na_2O, and Li_2O) connected to form a continuous transient melt, but the gas from the gas-evolving reactions had not begun to accumulate and expand the volume of the pellets [18, 19]. As discussed previously [6], the temperature at which the volume of the pellet reached a minimum, referred to as the foam onset temperature (T_{FO}), occurred at higher values for the feeds of increasing glass viscosity ($\eta_{A191\_75} < \eta_{A19\_75} < \eta_{A199\_75}$) and are listed in TABLE V. Since the lower viscosity feeds ($\eta_{A191\_75} < \eta_{A19\_75} < \eta_{A199\_75}$) had higher fractions of the low-temperature melting chemicals (H_3BO_3, Na_2CO_3, and Li_2CO_3), they reached the T_{FO} at a lower temperature.

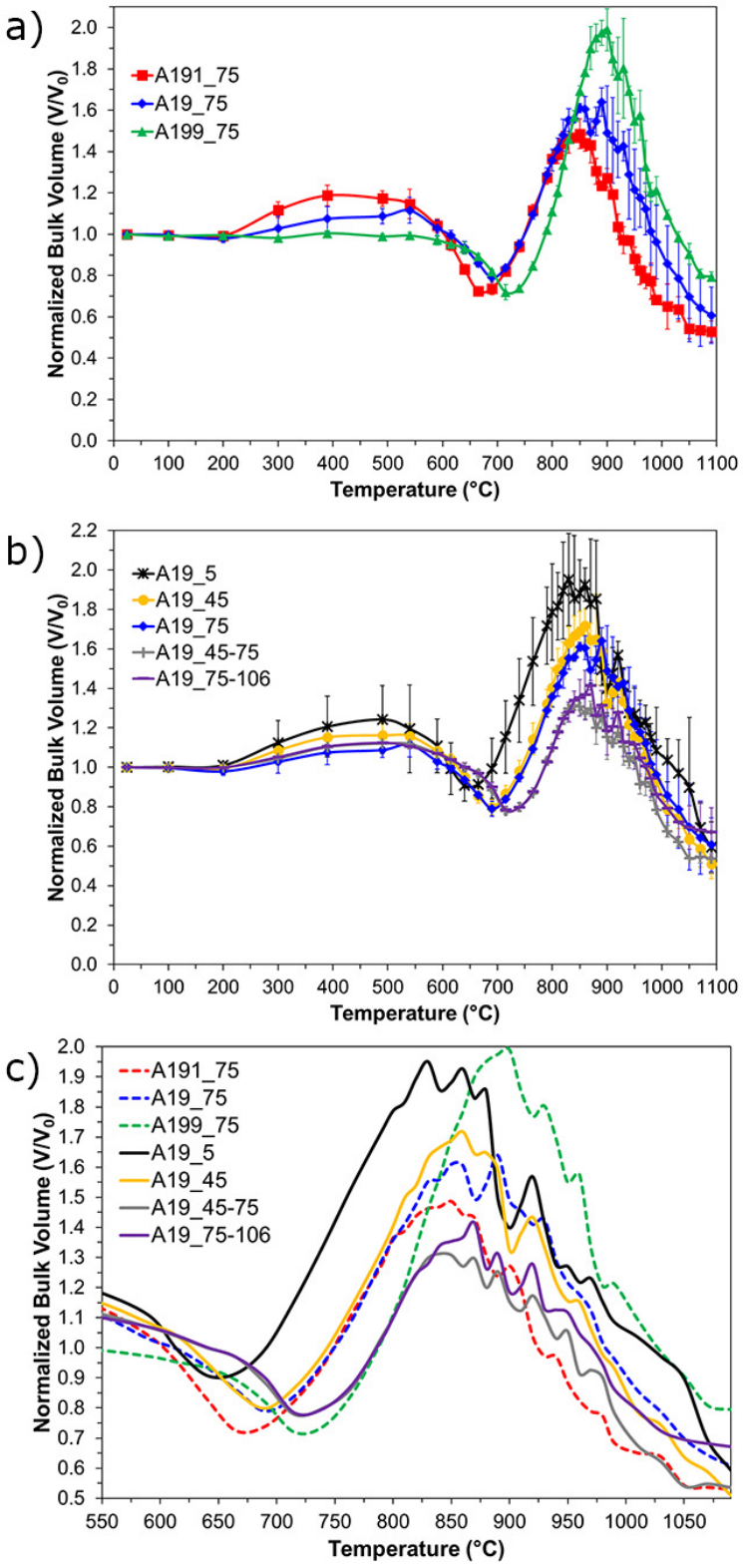

Fig. 1. a) Normalized bulk volume of A191_75, A19_75, and A199_75. b) Normalized bulk volume of A19_5, A19_45, A19_45-75, and A19_75-106. c) Normalized bulk volume of all feeds above 550°C.

TABLE V. Volume Expansion Characteristics

Feed Name	T_{FO} (°C)	V_{max}/V_0	T_{FM} (°C)
A191_75	672	1.486	848
A19_75	694	1.610	856
A199_75	724	1.990	898
A19_5	650	1.951	829
A19_45	691	1.718	858
A19_45-75	719	1.313	844
A19_75-106	720	1.416	869

After the T_{FO}, the volume of the pellets increased drastically as the residual gases became trapped by the newly connected melt. The maximum normalized bulk volume of the pellets (V_{max}/V_0), shown in TABLE V, increased for the feeds of increasing glass viscosity ($\eta_{A191\_75} < \eta_{A19\_75} < \eta_{A199\_75}$), which demonstrated that more gas was trapped in the more viscous melts.

Fig. 1b shows the volume expansion of the A19 feeds with various silica particle size fractions and TABLE V lists the T_{FO} and V_{max}/V_0 values for these feeds. Feeds A19_45-75 and A19_75-106, those without fine silica particles, expanded similarly, and so did feeds A19_45, A19_75, with silica fines. Fig. 1c summarizes all volume expansion curves over the temperature range of 550°C – 1090°C. The feeds with fine silica particles absent, A19_45-75 and A19_75-106, initially expand like the high viscosity feed A199_75, but reached a low maximum volume comparable with that of the low viscosity feed A191_75, which was a result of the slow dissolution of larger silica particles and thus a lower mass fraction of silica in the melt at maximum pellet volume. The melt with a low fraction of dissolved silica had a lower viscosity, thus causing a less stable foam [7, 9]. Unsurprisingly, the A19 feed with primarily fine silica particles (A19_5) expanded to maximum volume comparable to the high viscosity feed (A199_75), though at a lower temperature (foam maximum temperature, T_{FM}), as shown in TABLE V. The fine silica particles began to dissolve at lower temperatures resulting in a higher mass fraction of silica in the melt and thus a higher viscosity for trapping gases. The A19 feeds with both fines and larger silica particles (A19_45 and A19_75) fell in between the extremes of the low and high viscosity feeds.

During the charging of the feeds into the LSM crucible, videos showed gas cavities escaping around the perimeter of the cold cap. The observed cavities, large (~1.5-3 cm diameter) and small (~0.5-1.5 cm diameter), were counted on a per minute basis. Fig. 2 shows the frequency of total cavities (large plus small cavities) during charging. As noted previously [6], the size of cavities increased and the frequency of cavity escape decreased as the viscosity of the feeds increased ($\eta_{A191\_75} < \eta_{A19\_75} < \eta_{A199\_75}$). The low frequency of cavities escaping from the A199_75 cold cap towards the end of the charging time (25 and 30 minutes) could be attributed to

the massive foam layer observed in the cold-cap cross section of the high-viscosity sample [6]. The cavity escape frequencies for feeds with varying silica fraction did not appear to correlate with the varying viscosity regardless of initial silica particle size.

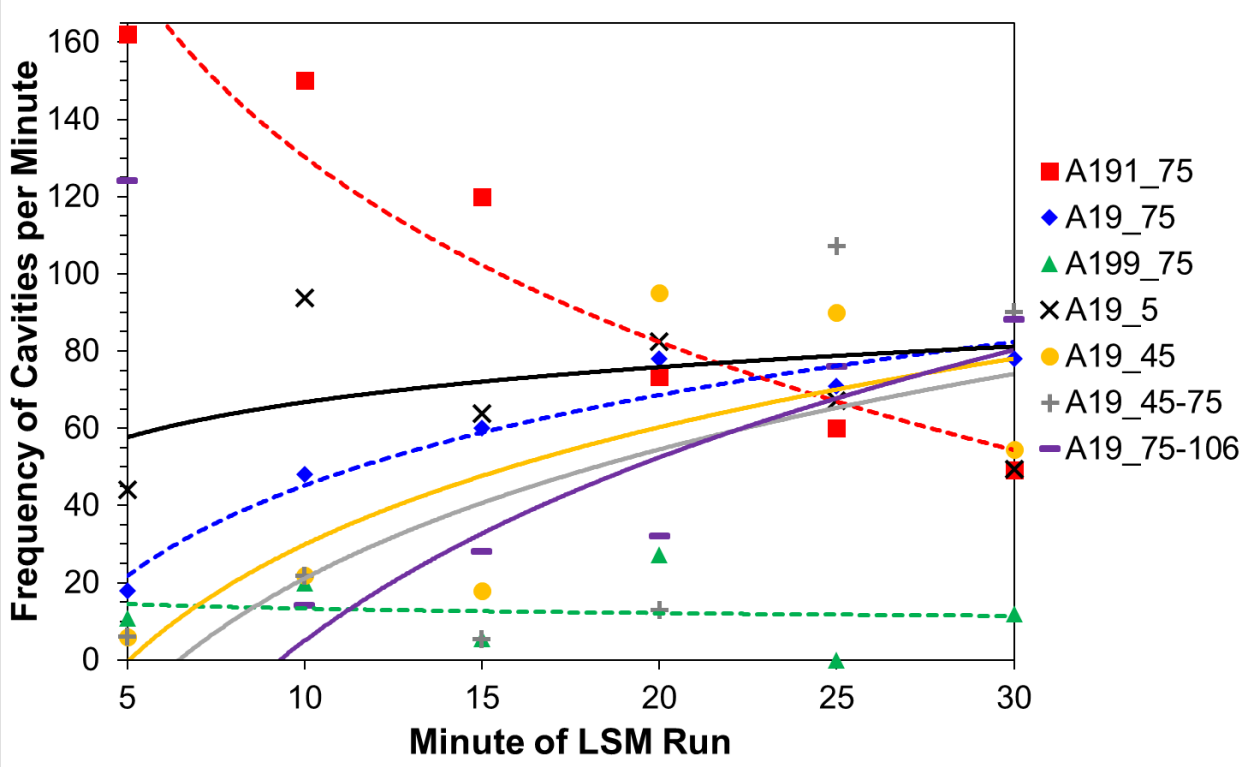

Fig. 2. Frequency of gas cavities escaping around the cold cap during charging of feed. The lines between points are drawn as a guide for the eye.

The quenched cold cap for each feed run in the LSM was photographed and the cold-cap top area was traced as shown by the white outline in Fig. 3a. The cold-cap coverage, Fig. 4, was determined by dividing the cold-cap top area by the LSM crucible area (70.9 cm^2). Each cold cap was then split along the existing fracture surface to reveal the profile through the cold-cap center. The height was measured at ~7 mm intervals along the profile, as shown in Fig. 3b. Fig. 4 shows the average heights. The cold cap volume was estimated as the product of area and height.

Whereas silica particle size and melt viscosity had pronounced effects on the feed expansion behavior revealed by the heated pellets (Fig. 1), the evolution of LSM-generated cold caps during feed charging appeared similar for each feed except for A199_75 feed in which the high-viscosity melt hindered the release of cavities, creating ~1 cm foam layer [6]. A similar foam layer was found under the A19_5 cold cap. These feeds exhibited high expansion as seen in Fig. 1.

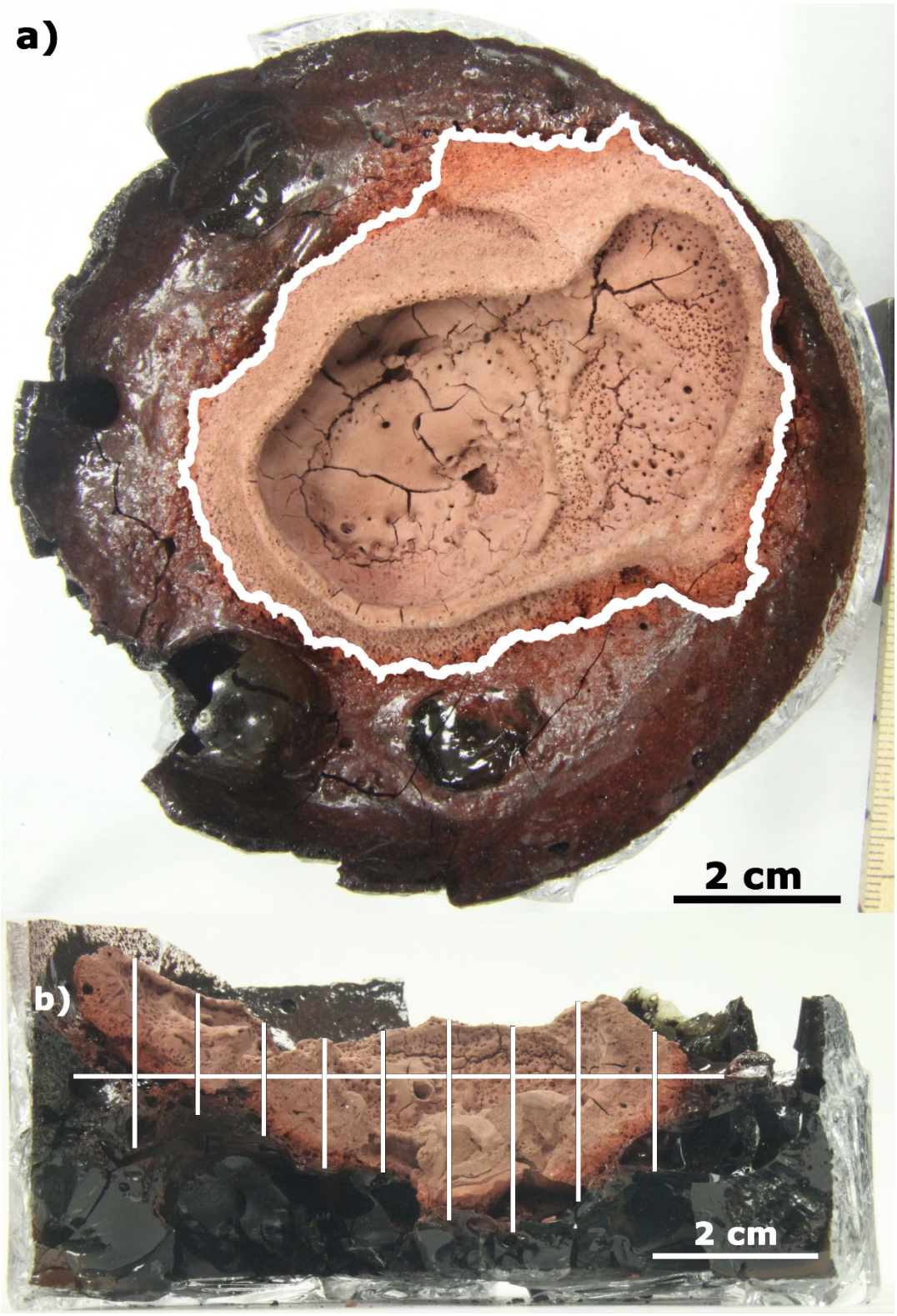

Fig. 3. a) A19_5 cold-cap top area traced by the white line and b) cold-cap height including cavities (measured at the locations of the vertical white lines).

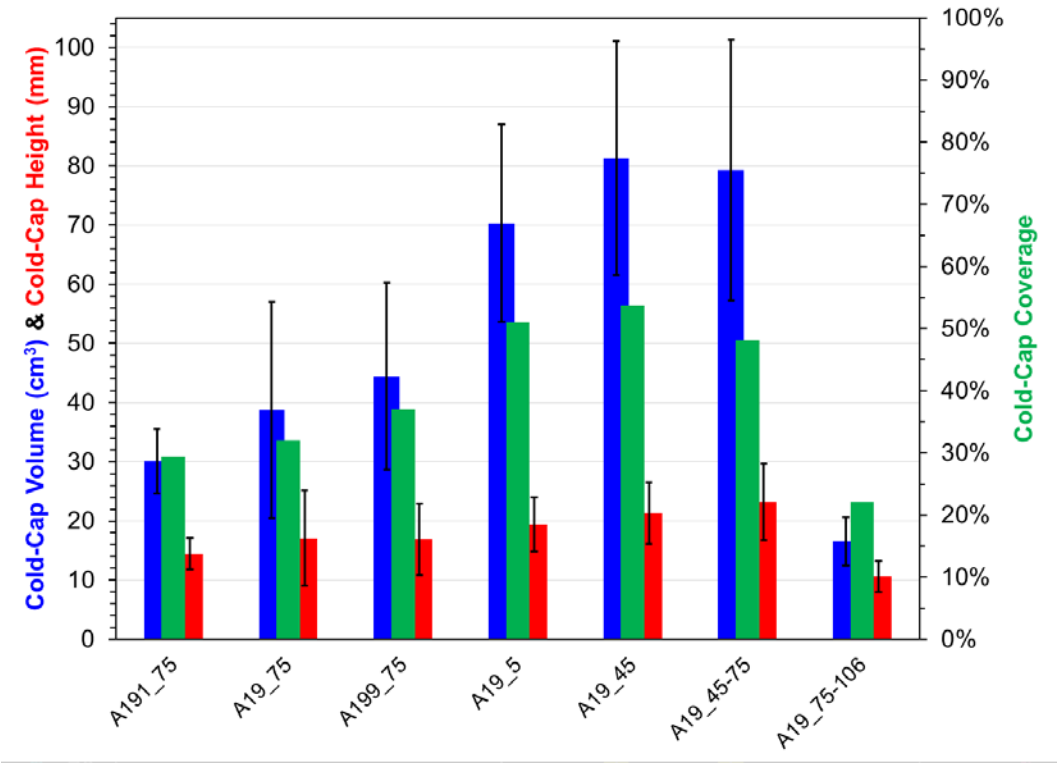

Fig. 4. Cold-cap volume, average height, and coverage (cold-cap top area divided by the LSM crucible area) for the feeds listed in TABLE III.

CONCLUSIONS

A high-alumina HLW feed composition was modified to create three feeds with differing glass viscosities. Four additional feeds were made by varying the size of the silica particles. The volumetric response of feeds to increasing temperature was recorded. The feeds batched as slurries were charged into a LSM. The movement of cavities around the cold cap during charging and the structure of the cold cap after quenching were observed. As the early-melt forming components connected the feed into a transient melt, the feeds without fine silica particles behaved similarly to the high viscosity feed, while the feed with silica particles no larger than 5 µm performed like the low viscosity feed. However, once gases became trapped in the transient melt, these relationships reversed and the feeds without fine silica particles behaved similarly to the low viscosity feed, while the feed with silica particles no larger than 5 µm performed like the high viscosity feed.

REFERENCES

1. BECHTEL NATIONAL INC, "About The Project," http://www.hanfordvitplant.com/page/the-project/ (2015).
2. P.J. CERTA, P.A. EMPEY, M.N. WELLS, "River Protection Project System Plan," ORP-11242 Rev. 6, U.S. Department of Energy Office of River Protection, Richland, Washington (2011).

3. D.K. PEELER, J.D. VIENNA, M.J. SCHWEIGER, K.M. FOX, “Advanced High-Level Waste Glass Research and Development Plan,” PNNL-24450, Pacific Northwest National Laboratory, Richland, WA (2015).
4. R. POKORNY, P. HRMA, "Model for the conversion of nuclear waste melter feed to glass," Journal of Nuclear Materials, 445, 190-199 (2014).
5. R. POKORNY, Z. HILLIARD, D.R. DIXON, M.J. SCHWEIGER, D.P. GUILLEN, A.A. KRUGER, P. HRMA, “One-Dimensional Cold Cap Model for Melters with Bubblers,” Journal of the American Ceramic Society, 98, 3112-3118 (2015).
6. D.R. DIXON, M.J. SCHWEIGER, S. LEE, J.S. HEILMAN-MOORE, P. HRMA, “Effect of Feed Composition on Cold-Cap Formation in Laboratory-Scale Melter,” WM2016 Conference, Paper#16336, Phoenix, AZ (2016).
7. S. LEE, Z. HILLIARD, J.S. HEILMAN-MOORE, D.R. DIXON, P. HRMA, M.J. SCHWEIGER, “The Effect of Quartz Particle Size and Melt Viscosity on HLW Melter Feed Pellet Test Response,” WM2016 Conference, Paper#16226, Phoenix, AZ (2016).
8. P. HRMA, J. MARCIAL, K.J. SWEARINGEN, S.H. HENAGER, M. SCHWEIGER, N.E. TEGROTENHUIS, “Conversion of batch to molten glass, II: Dissolution of quartz particles,” Journal of Non-Crystalline Solids, 357, 820-828 (2011).
9. M.J. SCHWEIGER, P. HRMA, C.J. HUMRICKHOUSE, J. MARCIAL, B.J. RILEY, N.E. TEGROTENHUIS, “Cluster formation of silica particles in glass batches during melting,” Journal of Non-Crystalline Solids, 356, 1359-1367 (2010).
10. J. MARCIAL, J. CHUN, P. HRMA, M. SCHWEIGER, "Effect of Bubbles and Silica Dissolution on Melter Feed Rheology during Conversion to Glass," Environmental Science & Technology, 48, 12173-12180 (2014).
11. K.S. MATLACK, W. KOT, I.L. PEGG, I. JOSEPH, A.A. KRUGER, “DM100 and DM1200 Melter Testing with High Waste Loading Glass Formulations for Hanford High-Aluminum HLW Streams, Test Plan 09T1690-1,” ORP-44198 Rev. 0, Vitreous State Laboratory, Washington, DC (2009).
12. D.R. DIXON, M.J. SCHWEIGER, B.J. RILEY, R. POKORNY, P. HRMA, “Temperature Distribution within a Cold Cap during Nuclear Waste Vitrification,” Environmental Science & Technology, 49, 8856-8863 (2015).
13. D.R. DIXON, M.J. SCHWEIGER, B.J. RILEY, R. POKORNY, P. HRMA, “Cold-Cap Temperature Profile Comparison between the Laboratory and Mathematical Model,” WM2015 Conference, Paper#15591, Phoenix, AZ (2015).
14. D.R. DIXON, M.J. SCHWEIGER, P. HRMA, "Characterizing a High-Level Waste Cold Cap via Elemental and Structural Configuration," WM2014 Conference, Paper#14185, Phoenix, AZ (2014).
15. D.R. DIXON, M.J. SCHWEIGER, P. HRMA, "Effect of Feeding Rate on the Cold Cap Configuration in a Laboratory-Scale Melter," WM2013 Conference, Paper#13362, Phoenix, AZ (2013).
16. Z. HILLIARD, P. HRMA, “A Method for Determining Bulk Density, Material Density, and Porosity of Melter Feed During Nuclear Waste Vitrification,” Journal of the American Ceramic Society, (2015).
17. B.J. VANDERVEER, Z.J. HILLIARD, P. HRMA, D.K. PEELER, M.J. SCHWEIGER, “Comparison of High-Level Waste Glass Feeds Containing Frit and Glass Forming Chemicals,” WM2016 Conference, Paper#16154, Phoenix, AZ (2016).

18. K. XU, P. HRMA, J. RICE, B.J. RILEY, M.J. SCHWEIGER, J.V. CRUM, “Melter Feed Reactions at $T \leq 700°C$ for Nuclear Waste Vitrification,” Journal of the American Ceramic Society, 98, 3105-3111 (2015).
19. K. XU, P. HRMA, J. RICE, M.J. SCHWEIGER, B.J. RILEY, N.R. OVERMAN, A.A. KRUGER, “Conversion of Nuclear Waste to Molten Glass: Cold-Cap Reactions in Crucible Tests,” Journal of the American Ceramic Society, 99, 2964-2970 (2016).

ACKNOWLEDGEMENTS

This work was supported by the U.S. Department of Energy’s Waste Treatment and Immobilization Plant Federal Project Office under the direction of Dr. Albert A. Kruger. The Pacific Northwest National Laboratory is operated for the Department of Energy by Battelle Memorial Institute under contract DE AC05 76RL0 1830. The authors would like to thank David Peeler for his discussion about the WTP and advanced glass formulations and Richard Pokorny for his discussion about the cold-cap foam layer.